Title
RECOIL RANGE DISTRIBUTIONS OF HEAVY MASS PRODUCTS IN DEEP INELASTIC REACTIONS WITH GOLD AND URANIUM TARGETS

Author
Otto, R.J.

Publication Date
1977-08-01

Submitted to Physical Review C

LBL-6529 c.1
Preprint

RECOIL RANGE DISTRIBUTIONS OF HEAVY MASS PRODUCTS IN DEEP INELASTIC REACTIONS WITH GOLD AND URANIUM TARGETS

R. J. Otto, M. M. Fowler, and G. T. Seaborg

August 1977

Prepared for the U. S. Energy Research and
Development Administration under Contract W-7405-ENG-48

DISCLAIMER

Recoil Range Distributions of Heavy Mass Products in Deep Inelastic Reactions with Gold and Uranium Targets

R. J. Otto, M. M. Fowler,* and G. T. Seaborg†

Lawrence Berkeley Laboratory and Department of Chemistry, University of California, Berkeley, California 94720

August 1977

Abstract

Recoil range distributions have been measured for the elements between lutetium (at. no. 71) and astatine (at. no. 85) produced in heavy ion reactions of 420 MeV, 491 MeV, and 581 MeV ^{86}Kr with ^{197}Au, 686 MeV ^{86}Kr with ^{238}U, and 868 MeV ^{136}Xe with ^{197}Au; the relative yields were established by use of x-ray spectrometry. These elements have been identified in radioanalytical mass distribution studies and kinematic studies as deep inelastic and quasielastic transfer reaction products. For the uranium target reactions they form the mass distribution colloquially referred to as the "gold finger." The measured recoil range distributions for the gold target reactions are correlated with energy and angular distribution measurements made on the projectile-like fragments formed in deep inelastic reactions.

NUCLEAR REACTIONS: $^{197}Au(Kr,X)Y$, E_{Lab} = 420, 491, 581 MeV; $^{197}Au(^{136}Xe,X)Y$, E_{Lab} = 868 MeV; $^{238}U(^{86}Kr,X)Y$, E_{Lab} = 686 MeV. Measured Recoil Range Distributions for $72 \leq Z_y \leq 84$.

I. INTRODUCTION

Prompted initially by the hopes of synthesizing superheavy elements, the study and theory of very heavy ion reactions has developed significantly since the discovery of the "quasifission" reaction.[1] Theories[2-3] for explaining and unifying the main features of many heavy ion reactions currently focus on an impact-parameter-dependent interaction time of the composite system, the diffusion rates of nuclear matter in the intermediate complex, and on the balance of the coulomb repulsive force and the dissipative force as the heavy ion projectile and target come together to form an intermediate complex. The last consideration has been parameterized by Moretto,[3] using the ratio (E-B)/B, where E is the projectile energy and B is the coulomb barrier, and by Galin[5] using a modified Sommerfeld parameter.[6]

Mass distribution studies of the reaction of ^{84}Kr + ^{238}U[7] and ^{136}Xe + ^{238}U[8] revealed a distribution of products between lutetium (at. no. 71) and astatine (at. no. 85) colloquially referred to as the "gold finger." Based on mass balance arguments in the Xe + U report[8] these products were identified as deep inelastic transfer products originating from the target. We will use the term target-like, gold-like or uranium-like in this case, for deep inelastic products that do not undergo fission in the de-excitation processes.

An alternative explanation, suggested by Deubler and Dietrich,[9] is that the gold finger is formed by sequentially fast fission of the uranium target and fusion of one of the fragments to the heavy ion projectile. Since the theoretical calculations for these events were made for low-impact-parameter collisions, the fragments from such a mechanism might be expected to have an angular distribution very different from those expected for a deep inelastic reaction.

Recoil range measurements can provide information on the energy and angular distribution of nuclear reaction products.[10] Since this information for the heavy mass target-like reaction products is not available for heavy ion reaction studies, we have explored the usefulness of this technique as a complement to information obtained from measured mass yield distributions, as well as to the heavy ion reaction studies of the lighter projectile-like fragment.

One objective of the study was to measure the recoil range distribution of the gold finger products so that the possible recoil loss corrections could be made in the thick target mass yield distribution studies. A second objective was to evaluate the differential recoil range data from heavy ion reactions as a way to identify and study reaction mechanisms. One of the distinct features differentiating the complete fusion-fission reaction and the deep inelastic transfer reaction is the angular distribution. When a large amount of rotational angular momentum is imparted to the compound nucleus before it undergoes fission, the angular distribution of the fission fragments will approach $1/\sin\theta$. The deep inelastic reaction of 620 MeV ^{86}Kr[11,12] and 979 MeV ^{136}Xe[13] with ^{197}Au has been characterized by a sideways peaking in the angular distribution of the light projectile-like fragment. Furthermore, beam counter studies of the deep inelastic component in the Kr + Au reaction[12] showed that the sideways peaking in the angular distributions disappeared and that the angular distributions of the projectile-like reaction products became forward-peaked as the Z of the projectile-like fragment moved to larger values farther away from the Z of the projectile. Since few angular distribution studies of the heavy target-like fragments have been made showing a complementary characteristic angular distribution, a third objective was to evaluate and use the recoil range method as a way to study the angular distributions of the target-like reaction products, particularly in the angular regions not covered by the beam counter studies.

The recoil ranges of heavy target-like products emitted at small angles in the c.m. system are easily measured. This corresponds to a region that is often inaccessible in counter studies of the complementary projectile-like products and thus recoil range data should potentially provide new information about heavy ion reaction mechanisms.

We have chosen to study the Kr + Au and Xe + Au reactions as a test of our method; first because of the availability of counter studies[11-13] and mass distribution measurements[14] that have been made on these two systems; second, because of the dominance of the deep inelastic reaction mechanism for these systems; and third, because of the stability against fission of the target-like products. The products between lutetium and astatine are formed both in the quasielastic transfer reaction, characterized by a very narrow mass distribution about the target, and in the deep inelastic transfer reaction, characterized by a broad mass distribution extending from the light rare earth region up to and beyond astatine.

In Sec. IV we show by comparison with counter data that the important features directly observed for the quasiprojectile fragments in the Kr + Au[11,12] and Xe + Au[13] reactions can also be deduced indirectly by proper interpretation of the recoil range data for the target-like fragments. In addition, angular distributions in regions not covered by the kinematic data are deduced. We also show that the angular distribution for the gold finger products from the Kr + U reaction are side peaked and that there is a correlation with the 620 MeV Kr + Au angular distributions as predicted, by using Galin's modified Sommerfeld parammeter.[2,5] Thus we have direct evidence for association of the gold finger products, with the deep inelastic reaction.

II. EXPERIMENTAL PROCEDURES

A. Target geometry and bombarding conditions

A stacked foil arrangement was used and a schematic diagram of the target and catcher foils is shown in Fig. 1. The targets consisted of 2.3 mg/cm^2 golf leaf foil, or approximately 1 mg/cm^2 of uranium as UF_4 on 1 mg/cm^2 aluminum backing. The uranium targets were prepared by vacuum evaporation of UF_4. These target foils were placed directly onto and in front of a stack of 1.0 to 1.1 mg/cm^2 aluminum recoil catcher foils. Aluminum recoil catcher foils were placed in front of the target whenever there was a possibility of recoiling fragments escaping from the target into the backward hemisphere. Table I gives a summary of the experiments and bombarding conditions. The energy drop in the targets ranged between 3% and 9% of the incident beam energy. Most of the experiments were run under parasitic conditions (i.e., as an adjunct to the experiments of a primary investigator). These targets and catcher foils were placed in the faraday cup of the scattering chamber of the primary user. The bombarding energies in Table I are the energies at the center of the target.

B. X-ray counting

Following the irradiation, the catcher foils and target were removed from the target holder, separated and individually taped to aluminum plates. The target and catcher foils were then analyzed for x rays with energies between 10 and 200 keV using a thin window intrinsic germanium detector under constant geometry conditions. In this way neither the absolute nor relative efficiency for the geometry used needed to be known. The maximum efficiency obtainable was 2%. The energy calibration of the x-ray system was determined by measuring the radiations from ^{241}Am and ^{207}Bi. The energy resolution of the system was 650 eV FWHM. The decay of the observed x-ray peaks in one of the foils showing strong x-ray activity was followed during the counting interval. Typically the counting was started several hours after the end of the irradiation. This allowed time for short-lived beta activity, primarily from spallation and transfer reactions of the heavy ions with aluminum, to decay. The beta activity added significantly to the compton background in the spectra and was the primary cause for the deadtime with the long range foils.

The irradiation times were, in almost all cases, longer than the total counting interval. These long low-intensity irradiations favored the formation of long-lived isotopes for each of the elements. Both short-lived components of a few hours and long-lived components of several days were seen. The decay data from the decay curves when taken over a long period of time, however, were statistically too uncertain to be analyzed for isotope identification. Due to the bombarding conditions and decay characteristics, isotopes of a few hours to a few days were approximately equally represented in the x-ray spectra.

Since the decay of only one of the recoil foils was followed, the empirical decay correction made for each of the other foils assumes that the isotopic distribution was the same in all recoil foils. Also, since the charge distributions are summed into a few of the long-lived (several hours to a few days) isotopes of each of the elements, rapid changes in the mass distribution if present could cause the recoil range distributions to be highly dependent on the decay characteristics of the few isotopes contributing to the x-ray peak of an element. This would result in noticeable irregularities in the recoil range distributions between elements. However, these irregularities were not seen. Errors in the decay correction are likely to be small since the time between the end of the bombardment and the start of the counting interval was in most cases greater than the length of the counting interval. Therefore, any isotopes with half-lives short compared to the counting interval would have decayed before the counting started.

III. RESULTS

A. X-ray spectra

X-ray spectra of the third recoil catcher foil, which usually contained most of the x-ray activity, are shown in Fig. 2 for each of the reactions studied. In the region from lutetium to astatine, 54 keV to 81 keV, the $K_{\alpha 1}$ x ray of any given element and the $K_{\alpha 2}$ x ray of the element of the next higher Z have differences in energies that are small compared to the resolution of the detector system. Thus a set of well-resolved peaks can be seen in this region consisting of overlapping $K_{\alpha1}$ and $K_{\alpha2}$ lines from adjacent elements. No x rays were ever seen corresponding to elements above polonium because of the short half-lives of most of the isotopes in the region between polonium and thorium or because of low yields in the uranium and transuranium region for the gold target reactions. The K_{β} x rays from the elements around and above gold do become significant and appear at energies greater than the mercury $K_{\alpha1}$ x-ray energy.

There are several factors contributing to the lack of clearly distinguishable x-ray peaks corresponding to elements in the rare earth region. The first is a combination of nuclear half-life systematics resulting in a relatively few number of detectable nuclides between cerium and lutetium. A second factor is characteristically lower production cross sections in this region, which represents near symmetric mass division of the composite systems of the reactions used in this study. Finally, the energies of the $K_{\alpha1}$ and $K_{\alpha2}$ x-ray lines do not overlap between adjacent elements and the resolution of the detector is insufficient to clearly resolve x-ray peaks in this region.

The x-ray spectra from the Xe + Au reaction show clearly for the first time structure in both the projectile-like and target-like region. The relative intensities of the x rays in the $^{86}Kr + ^{197}Au$ spectrum in Fig. 2 form qualitative pictures of the mass distribution for the products extending from lutetium to thallium that are nearly quantitatively consistent with thick target mass distributions determined by gamma-ray analysis for the same reaction.[14] However, the relative intensities of the x rays in the uranium reaction in Fig. 2 do not quantitatively reflect the distribution of mass in the gold finger region as determined by gamma-ray analysis in the thick target mass distribution experiments.[7,8] The explanation of these differences could be related to differences in the charge and mass distribution of the reaction products from thick and thin targets, the decay properties of these products, and production saturation effects favoring the longer-lived isotopes.

For the gold target reactions the quasielastic transfer products make some contribution to the x-ray activity of the elements near the target. However, the quasielastic products tend to have charge and mass similar to those of the target nucleus so that some will undergo negative beta particle decay and not produce x rays. The dominant contribution to the x-ray activity would be from the neutron deficient products formed in the deep inelastic reaction. The products in the hafnium to bismuth (or higher) region from the uranium reaction are too far removed in Z and A from the uranium target to be quasielastic transfer products. Since these "gold finger" products are very neutron deficient, they would rapidly undergo decay by electron capture or by alpha particle decay to longer-lived isotopes of lower Z that also undergo electron capture decay producing x rays.

B. Analysis of x-ray spectra

To determine the recoil range distribution from the x-ray data, each of the peaks was first identified with one of the elements in the hafnium to bismuth region based on the peak energy. Since the relative intensity of the $K_{\alpha 1}$ and $K_{\alpha 2}$ lines is approximately 2 to 1, unwanted gamma-ray contributions in a sequence of x-ray spectra would be recognized because they resulted in unacceptable intensity ratios. Recoil distributions were not calculated for the peaks where gamma-ray contributions intervended. The area under the x-ray peak was calculated by integrating the counts between the minimum points on either side of the peak. The compton background was calculated by using a linear interpolation between the minimum points. Once the area under each of the peaks in every spectrum was determined and the count rates calculated, correction for decay was made based on the measured decay in one of the foils. Since all of the reaction products were caught in one or another of the recoil foils, the fraction of the total activity of each of the observed elements in each recoil foil at the beginning of the counting interval could be obtained. What may be called the <u>differential axial recoil range distribution</u> for each element identified was then calculated by plotting the percent activity per recoil foil as a function of the axial range of the fragment.

The recoil range distribution plots shown in Figs. 3-11 can be understood as follows. There is one range distribution derived for each x-ray peak identified in the x-ray spectra. The ordinate labeled "Percent (of Recoil Product Activity) Per Recoil Foil" represents the relative number of atoms in each recoil foil of the two elements corresponding to the identified x-ray peak. Each aluminum recoil foil has a finite thickness represented in the figure by the width (in mg/cm^2) of the bar. Also, each recoil foil in the stack corresponds to upper and lower limit axial recoil range depending on its position in the recoil stack. Thus, these recoil range plots show the distribution of the reaction products among the foils expressed as a function of their axial range with a resolution equal to the thickness of the aluminum recoil foils. The resulting axial recoil range distributions from the reactions studied for elements between hafnium and polonium are shown in Figs. 3, 4, and 5. When the peak area was less than the uncertainty associated with the compton background, upper limits were set equal to one standard deviation in the compton background in the region in which the peak would be expected to be observed.

C. Methods of analysis of recoil range distribution

The most striking feature in the range distribution (compare Figs. 3, 4, and 5) is the similarity of the differential recoil range distributions among the elements for a given bombarding energy and reaction. This similarity spans a much broader region of elements than would be expected for the span of elements contributing to a single recoil range distribution through growth and decay in an isobaric decay chain. Thus these curves reflect the kinematic properties of the primary products produced in these heavy ion reactions.

To make a more complete analysis of the measured recoil range distributions and correlate them with the kinematic studies of the complementary light projectile-like fragments, a simplified reaction model was chosen. Using this model a computer code was written that could be used to calculate a theoretical recoil range distribution for the given reaction under the experimental conditions.

Beam counter studies of the projectile-like products in the quasi-fission or deep inelastic reaction of krypton with gold[11,12] targets have shown, to first approximation, that for this target and projectile combination the average energies of the fragments correspond to the coulomb repulsion energy of two touching spheroids. Second, it has been shown that the average c.m. energy is independent of the angle of emission. Our reaction model includes these observations.

In this model the reaction is assumed to occur in two steps. In the first step the projectile collides with the target nucleus. The relative motion of the target and projectile is assumed to be completely damped into internal excitation energy of the combined target-projectile system. The target and projectile are effectively merged together for some time, referred to as the interaction time, that may be long or short compared to the rotational period of the system. The laboratory velocity of the c.m. system $V_{c.m.s}$ is determined by the momentum conservation equation used for compound nucleus reactions, $M_pV_p = (M_p + M_t)\ V_{c.m.s}$. During the interaction time nucleon exchange and excitation energy equilibration between the two temporarily merged fragments takes place. The extent of the interaction may vary from the net transfer of one or two nucleons to the formation of a compound nucleus (complete fusion). In the second step the merged system separates into two fragments. The velocity of the fragments is determined by the coulombic energy of two touching spheroids. At this point it would be possible to add an initial dynamical fission energy or to reconvert the orbital rotational angular momentum of the system into additional translational motion of the two fragments. Neither of these two additional energies was used at this time in these calculations. The final separated fragment velocities are assumed to be independent of the c.m. angle at which they are emitted.

The light and heavy fragments are emitted directly opposite each other in the c.m. coordinate system, so that the emission angles and the angular distribution probabilities are complementary. For a fully damped collision each of the fragments contains a fraction of the total excitation energy (minus the separated fission kinetic energy) that is proportional to its mass. Particle evaporation will result in small angular deviations for the heavy fragment from its initial direction; therefore, these corrections have not been made in the recoil calculations.

The exact methods and formulas used to calculate the theoretical recoil range distribution and the values R_{max}, R_{min}, R_{90} and R_g under the experimental conditions is described in Appendix A. R_{max} corresponds to the maximum target-like fragment range being emitted to 0° in the c.m. system. Thus the coulomb repulsion velocity and velocity of the c.m. are aligned. R_{min}, the minimum target-like range, results from the coulomb repulsion velocity and velocity of the c.m. being opposed for the heavy target-like fragment. The range for a product emitted at 90° in the c.m. coordinate for a fully damped collision is represented as R_{90}. For an angular distribution symmetric about 90° (c.m.s) such as an isotropic or a $1/\sin\theta$ type angular distribution expected for fusion-fission reactions, half of the recoiling products should have ranges longer than R_{90}. The axial range of a product emitted at the classical grazing angle in the c.m. system for the fully damped deep inelastic reaction is represented by R_g. These ranges, R_{max}, R_{min}, R_{90}, and R_g calculated for the indicated products produced in the reactions studied, are given in Table II.

Our calculations predict differential axial recoil range distributions that are distinctly different for different angular distributions. As an example, Fig. 6 shows three hypothetical angular distribution for the complementary light fragment and the corresponding recoil range distributions for gold fragments from the reaction of 581 MeV $^{86}Kr + ^{197}Au$. Furthermore, changing the coulomb repulsion energy of the two fragments by adjusting r_0 between 1.0 and 1.4 had little effect on the relative shape of the calculated range distributions. For fully damped reaction mechanisms the range distributions primarily reflect the angular distribution. Figure 6 also indicates that a small $1/\sin\theta$ component, possibly associated with a compound nucleus reaction, would cause a significant fraction of the activity to have the maximum range, $R_{max} \approx 7$ mg/cm^2, contrary to the experimental results. An alternative to the above calculations would be to deduce the angular distribution from the recoil range data for a given element. It is possible to do this in a somewhat straightforward manner if the kinetic energy of the fragment is considered to be constant in the c.m. system, and the thickness of the target is not taken into account. A simple way to visualize the relationship between the axial recoil range distribution and the angular distribution, $(d\sigma/d\theta)$, is to imagine that the probabilities of finding a given product in the three dimensional coordinate space around the target are projected onto a line defined by the beam axis. These probabilities summed over distances equal to the thickness of the recoil foils are just the axial recoil range distribution. Using the same formulas given in the appendix, it is possible to associate each axial recoil range with a c.m. angle. In this way, the angular distribution (in relative units) has been calculated directly for some of the products from the $^{86}Kr + ^{197}Au$ reaction (see Fig. 7).

There are several errors introduced into the recoil range calculation. First, only the range corresponding to the average fragment energy is calculated when in fact the fragment energy distributions are broad and asymmetric. This effect should be averaged out to some extent in the calculation for smooth and slowly varying angular distributions. Second, the recoil range is calculated for a single isotope of each element, chosen by assuming charge to mass equilibration of the two fragments, when in fact the experimental range distributions come from broad charge distributions and irregular contributions from nearby elements due to growth and decay. In addition, neutron evaporation effects from the primary fragments, although expected to be small, are not taken into account. Also, the range energy relationship for very neutron deficient fragments is not well known. The calculated ranges are based on the Northcliffe Schilling[15] range values and these values are thought to be 10% too large.[16] Multiple scattering effects have been estimated to cause deviations of $\pm 10°$ about the emission angle, and this effect along with recoil range straggling will also add some small error to the calculation. In spite of these shortcomings in the model and calculations, we have found by comparison with experimental data that the measured and calculated recoil range distributions are sensitive to the major features of the reaction mechanism being studied.

IV. COMPARISON OF EXPERIMENTAL AND CALCULATED RECOIL RANGES

A. Kr + Au

The majority (50% to 80%) of the activity in each of the recoil range distributions in Fig. 3 is in just two of the 1 mg/cm^2 recoil catcher foils. In Fig. 7 a comparison is made of typical recoil range distributions for each of the three bombardments. The most probable range in each distribution is at or slightly less than R_g, indicating that the angular distribution associated with these products is sideways peaked at or near the grazing angle consistent with the kinematic studies. Shown to the right of the recoil range distributions are the angular distributions ($d\sigma/d\theta$) for the Pt(Au) products deduced from these range distributions as described in the previous section. It can be seen in this figure that the peak in the angular distribution is near the calculated grazing angle for the heavy fragment.

In the Kr + Au reactions the most probable range of the products increases as the bombarding energy decreases. This effect is clearly seen in Fig. 7. This experimental trend of increasing range of the target-like product with decreasing energy of the projectile can be correlated with the shift of the peak in the angular distributions of the projectile-like products to larger angles as the bombarding energy decreases. This trend was first reported in a study of the reactions of Kr with lead targets.[17,18] The angular distributions of the krypton-like products in these reactions was sideways peaked. As the bombarding energy decreased the peak moved toward larger angles, following the same trend in the grazing angle, and the peak width broadened. Since the reaction is a binary process the focused angular distribution of the krypton-like products results in a complementary focused angular distribution of the gold-like products reflected by 180° in the c.m.s. As the angular distribution peak of the krypton-like products moves to larger angles in the c.m. system, the gold-like products angular distribution peak must move to smaller angles (closer to 0°) resulting in longer axial ranges, exactly as observed in Figs. 3 and 7. Thus the peak in the angular distribution of the projectile-like component is correlated with the peak in the recoil range distributions of the target-like products.

We have also used the measured angular distributions of the krypton-like fragments from a study of the reaction of 620 MeV ^{86}Kr + ^{197}Au[11,12] to predict the recoil range distributions of the complementary quasigold products for the same reaction at our slightly lower bombarding energy of 581 MeV. Figure 8 (left side) shows the experimental angular distribution data for the krypton-like products[11,12] and a smooth angular distribution function fit through these data used as input for the calculation. Figure 8 (right side) shows that there is a good fit of the calculated and measured recoil range distributions for the gold-like fragments. These comparisons show that the recoil calculations provide a way to identify and determine the major features of the reaction mechanism associated with the recoil range distributions.

To reproduce the experimental recoil distribution shapes for ranges beyond 3 mg/cm^2, an exponentially decreasing angular distribution of the projectile-like component between 120° and 180° was assumed and used in the calculation. This is the angular region where there were no measurements of the angular distributions for the light krypton-like fragments. Calculating the range distribution using a small $1/\sin\theta$ (actually $1/[\sin\theta + 0.01]$) component in the angular distribution requires a significant fraction of the activity to have ranges corresponding to 6 to 8 mg/cm^2 (see Fig. 6). This does not correspond to the experimental data. No evidence for such a component can be seen in the 581 MeV Kr + Au reaction, even though as little as 5% of the reaction mechanism having a $1/\sin\theta$ component for these products would have been detectable in these recoil range distributions.

B. Xe + Au

The measured recoil range distributions for the reaction of 868 MeV Xe + Au are shown in Fig. 4. For comparison, the calculated values R_{min} R_g, R_{90} and R_{max} values are displayed in Fig. 9 with the measured recoil range distribution for the elements Re(Os). The peak of the range distribution corresponds to R_g, indicating that the angular distributions for the complementary xenon-like products are peaked at or near the grazing angle. The angular distributions for the xenon-like products have in fact been measured for a limited angular range for the reaction of 979 MeV ^{136}Xe + Au[13] and found to be relatively narrow, and peaked at the grazing angle. Figure 9 shows a comparison of the calculated range distributions using the measured angular distribution widths for the Xe + Au reaction. The experimental range distribution probability for the target-like products Re(Os) is much broader, extending to longer ranges than the calculated range distribution. This contrasts with the better fit for the Kr + Au reaction in Fig. 8, where the asymmetric shapes of the distributions result from asymmetrically shaped angular distributions of the projectile-like fragments. These angular distribution shapes and trends for the Kr + Au reaction are correlated with long interaction times and a tendency toward forward peaking.[13] However, incomplete damping and shorter interaction times characterize the Xe reactions with Bi[19], Ta and Pb[20]. Thus the assumption of long interaction times and complete damping, which worked well for the Kr + Au case, apparently does not apply to the Xe + Au reaction. The range of the heavy fragment, corresponding to the light fragment being emitted at the grazing angle, is 4.2 mg/cm^2 for a purely elastic collision and 3.3 mg/cm^2 for a fully damped collision. The range for partially damped events would fall somewhere in between these values, resulting in an asymmetry of the type observed in Figs. 4 and 9.

Another feature seen again in the Xe + Au range distributions is the absence of any evidence for a $1/\sin\theta$ component in the angular distribution. This follows from the fact that no product x-ray activity was seen in recoil foils corresponding to ranges equal to R_{max}. The most interesting region to look for a $1/\sin\theta$ component would be at the mass symmetry point around dysprosium. The lowest mass number, corresponding to the largest mass diffusion from the target to projectile and therefore longest interaction times for which it was possible to obtain recoil range data, was for the element rhenium. The region of $Z \leq 75$ and particularly the region near dysprosium, which represents the mass symmetry point and longest interaction times for the two fragments, could not be explored because of significant interference of gamma-rays with energies near that of dysprosium x rays in the recoil foils beyond 3 mg/cm^2 of aluminum.

According to Moretto[3] the observed transition for the projectile-like fragments from side peaking to forward peaked angular distributions can be correlated with decreasing values of the ratio (E-B)/B. A survey of Table 1 shows that the (E-B)/B value for 491 MeV ^{86}Kr + ^{197}Au is most similar to the value for 868 MeV ^{136}Xe + ^{197}Au. Comparison of Figs. 3 and 4 shows that the shapes of the recoil range distributions are similar for both reactions, indicating similar angular distributions for the quasigold products for the two reactions. An effect common to both sets of range distributions is the broad widths of the recoil range distributions. This width was correlated for the Kr + Au reaction with broader peaked angular distributions for the complementary krypton-like products that result from increased interaction times. In contrast, the widths of the Xe + Au range distributions are correlated with incomplete damping corresponding to shorter interaction times. Moretto[3] shows that the (E-B)/B ratio is proportional to the product of the life time of the intermediate complex system and the rotational velocity which is larger on the average for the Xe + Au reaction. Although the similarity of the recoil range distributions for 868 MeV ^{136}Xe + ^{197}Au and 491 MeV ^{86}Kr + ^{197}Au would appear to support this interpretation of the ratio E-B/B, the analysis of the range data consistent with the other experiments previously mentioned, that suggest different degrees of damping in the deep inelastic reaction, indicate that the proper scaling parameter should include the viscosity, or dissipative effects, which are ignored in the above interpretation but which must play an important role. In the next section we discuss the η' parameter suggested by Galin.[5] The fact that this parameter and the ratio (E-B)/B are closely related, explain why they both qualitatively scale with the angular distribution trends. The η' parameter, however, is interpreted somewhat differently to include the dissipative frictional forces.

C. Kr + U

The recoil range distributions for the reaction of 686 MeV ^{86}Kr with ^{238}U are shown in Fig. 5. These products are part of the mass distribution identified as component G (the distribution colloquially referred to as the gold finger) in the Kr + U mass distribution.[7] Figure 10 shows that the range distributions are peaked at values slightly less than R_g, indicating an angular distribution side peaking of the complementary quasi-krypton fragment at angles slightly larger than the grazing angle.

Galin[5] has shown that the angular distributions for heavy ion reactions can be grouped into three categories; forward peaking ($\eta' < 210$), intermediate forward plus side peaking ($210 \leq \eta' \leq 280$), and side peaking ($\eta' > 280$). The scaling parameter η' is given by Eq. 1.

$$\eta' = \frac{Z_1 Z_2 e^2}{\nu'} = \frac{Z_1 Z_2 e^2 \cdot \mu}{\hbar (E-B)^{\frac{1}{2}}}. \qquad (1)$$

Z_1 and Z_2 are the atomic numbers of the target and projectile, ν' is the relative velocity of the fragments at the peak of the coulomb barrier, μ is the reduced mass of the system, and E and B are the c.m. bombarding energy and coulomb barrier, respectively.

The parameter η', as pointed out by Galin[5] and Lefort,[2] is proportional to the ratio of coulomb repulsive force and the dissipative frictional forces in the intermediate system. Thus one might expect the interaction times and angular distributions for two different heavy ion reactions such as ^{86}Kr + Au and ^{86}Kr + U to be similar under conditions in which η' is nearly the same. The calculated value of η' is 304 for 686 MeV $^{86}Kr + {}^{238}U$. The calculated value of η' is 283 for 620 MeV $^{86}Kr + {}^{197}Au$, close to the Kr + U value. Thus we expect the angular distributions for the deep inelastic reaction products for these two systems to be comparable. In Fig. 11 we have used the measured angular distributions of the projectile-like products from the 620 MeV $^{86}Kr + {}^{197}Au$[11,12] reaction to calculate recoil range distributions for the 686 MeV $^{86}Kr + {}^{238}U$ uranium-like recoil product Ir(Pt). Based on these Kr + Au angular distributions, the left side of Fig. 11 shows two possible angular distributions for the Ir(Pt) products from the Kr + U reaction. The solid line is deduced from the measured angular distribution from the 620 MeV Kr + Au reaction of the krypton-like products (Z = 37) that were complementary partners to the platinum products. The angular distribution corresponding to Ir(Pt) deep inelastic products taken from the Kr + Au data is converted to a range distribution for the Kr + U reaction and compared with the measured range distribution for these products. A better fit of the experimental range data is obtained with the dashed line angular distribution. This distribution is closer to the shape (again 180° reversed) of the distributions obtained for $Z \geq 44$ products ($\Delta Z \geq 8$) for the Kr + Au reaction. This is exactly what one expects since the Ir(Pt) products from Kr + U correspond to a $\Delta Z \cong 14$ transfer from the target to the projectile. Thus the majority of the Ir(Pt) gold finger products are associated with a weakly focused deep inelastic angular distribution. Since up to 12-20 protons must be transferred, and at least an equal number of neutrons, from the target to the projectile to form these products, long interaction times are required. Also since our results indicate there is little or no orbiting (no $1/\sin\theta$ component), these products must be formed in the more penetrating low impact parameter, low angular momentum collisions.

The suggestion that the gold finger products are formed by "fission followed by fusion" mechanism cannot be distinguished in these recoil range data. Low impact parameters are expected to lead to this type of reaction.[21] Thus the gold finger products would be formed by a combination of a forward moving (~0°) projectile and a backward moving (~180°) uranium fission fragment so that the final range of these fragments would be expected to be zero on the average. Short ranges do in fact characterize most of the recoil products formed in the $^{86}Kr + {}^{238}U$ reaction in agreement with the above conclusion. It is more reasonable, however, to associate the range distribution with the deep inelastic mechanism since the fission-fusion theory predicts very neutron excessive gold finger products contrary to what was found in the mass distribution studies.[8] It would be possible to test this theory, however, by lowering the projectile energy. The deep inelastic reaction mechanism would result in a shift of the peak in the range distribution plots to longer ranges, as in Fig. 7 for Kr + Au at 420 and 491 MeV. The fission-fusion mechanism should result in a small shift of the peak to longer ranges by assuming small impact parameters and using the arguments above.

IV. CONCLUSIONS

The method of measuring the recoil ranges of elements between lutetium and astatine using a stacked foil geometry and x-ray spectrometry has proven to be an experimentally simple and at the same time a useful method for studying heavy ion reactions of Kr and Xe with heavy targets. The recoil range data for these reactions show that the elements between lutetium and astatine are produced primarily by the deep inelastic transfer reaction mechanism. The recoil range distributions for the heavy target-like fragments from the Kr + Au reactions can be correlated with measured angular distributions of projectile-like fragments from the same or similar reactions using the simplified fully damped model. Partial damping of the Xe projectile in a deep inelastic collision with Au explains the long range tailing effect in the recoil range distributions of the gold-like products. The recoil range distributions of the products near gold from the Kr + U reaction indicate that the products have a predominantly side peaked angular distribution. The peak is near and below the grazing angle. Using the modified Sommerfeld parameter η' to equate the angular distributions of the two reactions (686 MeV ^{86}Kr + ^{238}U and 620 MeV ^{86}Kr + ^{197}Au), one would predict weakly side peaked angular distributions as indicated in the recoil range data.

The recoil range studies provide another dimension to mass distribution studies of heavy ion reactions that can be correlated with the kinematic studies of these same reactions. The Kr + U recoil range results provide direct evidence to support the conclusion reached in the report of the Xe + U mass distribution[8] concerning the mass distribution colloquially referred to as the gold finger observed for both the

Kr + U and Xe + U reactions. These products are primarily part of the uranium-like fragment distribution that deexcited by proton and neutron evaporation rather than by fission. The "fission followed by fusion" theory of Deubler and Dietrich has been considered. The measured range distributions for Kr + U do not provide a good test for the theory. However, the theory predicts neutron excessive "gold finger" products contrary to what was found in the mass distribution studies.

The recoil range method used in this study is a good way to identify the reaction mechanism or mechanisms associated with the production of heavy mass products between lutetium and astatine, provided the production reaction is a binary event. The use of this method in the study of even heavier projectile-target combinations such as the reaction of U + U should provide useful information about the reaction mechanisms responsible for the production of products between lutetium and astatine.

APPENDIX: CALCULATION OF RECOIL RANGE DISTRIBUTIONS

The recoil range distribution is calculated by a numerical summing process that can be made independent of the chosen reaction mechanism, but at the present time is restricted to the fully damped model described in the text. The initial variables for the kinematic calculation are specified for a given reaction. These variables are the mass and charge of the target and the mass and charge and laboratory energy of the heavy ion projectile. The atomic number of the heavy fragment for which a range distribution is to be calculated and the angular distribution for the light fragment in the c.m. system is also chosen. The target thickness and the thickness of each of the aluminum recoil foils is also given.

The reaction is considered to be a binary event, so the mass of the heavy fragment and the mass and charge of the light fragment are calculated first. No particles are assumed evaporated before the formation and separation of the light and heavy fragments. Mass to charge equilibration is assumed to take place and the mass and charge of the two fragments are then determined by the choice of Z_H

$$M_H = Z_H \cdot \frac{M_P + M_T}{Z_T + Z_P} \tag{A1}$$

$$Z_L = Z_T + Z_P - Z_H \tag{A2}$$

$$M_L = M_T + M_P - M_H, \tag{A3}$$

where the letters M and Z represent mass and atomic number and the subscripts P, T, H, L denote the projectile, target, heavy and light fragments, respectively.

The total kinetic energy of fission E_C is calculated next using the separation distance formula given in Eq. (A4) for two touching spheres.

$$R = [1.225\ (A_1^{\frac{1}{3}} + A_2^{\frac{1}{3}}) + 2]\ \text{fm}. \tag{A4}$$

Once the mass of the fragments is fixed and the total kinematic energy of fission calculated, the energies and emission angles of both fragments in the c.m. reference frame and in the laboratory can be calculated by choosing θ_L, the emission angle in the c.m. system for the light fragment. The relationship between the velocities of the fragments both in the laboratory and c.m. system are shown in Fig. 12. The following formulas were used to calculate the final energy and angle of the heavy fragments under the conditions specified:

$$V_{c.m.s} = (2\ M_P\ E_P)^{\frac{1}{2}} / (M_P + M_T) \tag{A5}$$

$$\mu = \frac{M_H\ M_L}{M_H + M_L} \tag{A6}$$

$$V_H = (2\ E_C \cdot \mu)^{\frac{1}{2}} / M_H \tag{A7}$$

$$\theta_H^{lab} = \arctan\left[\frac{V_H \sin \Psi_H}{V_{c.m.} + V_H \cos \Psi_H}\right] \tag{A8}$$

$$V_H^{lab} = \left[(V_H \cos \Psi_H + V_{c.m.})^2 + (V_H \sin \Psi_H)^2\right]^{\frac{1}{2}} \tag{A9}$$

$$E_H^{lab} = \tfrac{1}{2} M_H (V_H^{lab})^2, \tag{A10}$$

where Ψ is used to represent the emission angles in the c.m. system and θ the corresponding laboratory angles. μ is the reduced mass of the fissioning system and $V_{c.m.s}$ is the velocity of the center of mass of the reaction. Again subscripts P, T, H, and L refer to the projectile, target, heavy fragment and light fragment, respectively, superscripts c.m. and lab refer to the center of mass and laboratory reference frames, and V and M are used to denote velocity and mass.

Once the laboratory energy and angle of the heavy fragment have been calculated, its range in aluminum was calculated using a parameterization of the Northcliffe and Schilling[15] tables. The range for several elements in Al were fit to an equation of the form

$$R_{ref} = K_1 E_{ref} + K_2 \; [1 - \exp \; (- K_3 E_{ref}) \tag{A11}$$

where

$$E_{ref} = E_H^{lab} \cdot \frac{M_{ref}}{M_H} \tag{A12}$$

and M_{ref} is the mass of the same element, found in the range tables, as the heavy fragment with mass M_H.

The parameters K_1, K_2, and K_3 were fit to an empirical set of functions that depended on the Z of the fragment for which a range was to be calculated. The functional forms are given below where Z is the atomic number of the reference mass M_{ref} and the fragment mass.

$$K_1 = (10^{P_1 + P_2 Z}) \; / \; M_{ref} \tag{A13}$$

$$K_2 = (10^{P_3 + P_4 Z}) \; M_{Ref} \tag{A14}$$

$$K_3 = (10^{P_5 + P_6 Z}) \; / \; M^2_{Ref} \tag{A15}$$

The values sued for this parameterization were:

$P_1 = 0.36514$

$P_2 = 3.3287 \times 10^{-4}$

$P_3 = -1.7967$

$P_4 = - \; 1.8132 \times 10^{-3}$

$P_5 = 2.7082$

$P_6 = 3.3025 \times 10^{-3}$

To calculate the range of the fragment corresponding to E_H and M_H the value R_{ref} must be corrected.

$$R_H = R_{ref} \cdot \frac{M_H}{M_{ref}} . \tag{A16}$$

The final reference ranges are within ±5% of the values given in the range tables for elements between iodine and uranium.

The recoil range along the path of the fragment R_H and the axial range R_H are calculated for the heavy fragment for angles every 0.1° between 0° and 180° in the c.m. system.

$$R_H \text{ (axial)} = R_H \cdot \cos (\theta_H{}^{Lab}). \tag{A17}$$

The ranges are sorted into axial range intervals and the angular distribution probability $P(\theta)$, proportional to $d\sigma/d\theta$, is calculated and summed for each interval as the calculation proceeds.

$$P(\theta) = \sin \frac{d\sigma}{d\Omega} = \frac{d\sigma}{d\theta} . \tag{A18}$$

When the calculation has been completed for each of the 1800 c.m. angles the normalized probabilities in each bin represent the <u>differential axial recoil range distribution</u> for the element.

The entire calculation cycle from 0° through 180° is repeated for 10 separate depths in the target and the results normalized and summed. In this way the target thickness is taken into account. The target thickness is expressed as an equivalent thickness of aluminum by using the relationship in Eq. A19:

$$T_{Al} = T_{Target} \quad \frac{(dE/dx)_{Target}}{(dE/dx)_{Aluminum}} , \tag{A19}$$

where the differential energy losses are evaluated at 1 MeV/nucleon for a typical heavy fragment in the target material and in aluminum. The range probabilities can be summed for range intervals corresponding to the experimental recoil foil geometry and compared with the experimental results.

ACKNOWLEDGMENTS

We would like to express our thanks to Dr. Luciano Moretto and members of his research group for providing experimental time with their faraday cup and for helpful discussions. We thank Dr. Irwin Binder, Mrs. Diana Lee, and Mr. David Morrissey for their assistance. We also wish to express a special thanks to Mr. Robert Klein and Miss Elaine Dong for their assistance in analyzing the x-ray spectra and Mr. Klein's efforts in parameterizing the Northcliffe and Schilling tables.

REFERENCES

† Work supported by the Division of Physical Reseach of the U. S. Energy Research and Development Administration.

* Present address Los Alamos Scientific Laboratory, Los Alamos, New Mexico 87545

[1] F. Hanappe, M. Lefort, C. Ngô, J. Peter, and B. Tamain, Phys. Rev. Lett. 32, 738 (1974)

[2] M. Lefort, "Symposium on New Avenues in Nuclear Physics Rehovot (Israel)," Nov. 7-9, 1976.

[3] L. G. Moretto and R. Schmitt, European Conference on Physics with Heavy Ions, CAEN, J. Physiwue (1976).

[4] J. Huizenga, Comments on Nuclear and Particle Physics (1977).

[5] J. Galin, "European Conference on Physics with Heavy Ions," CAEN, J. Phys. Paris Colloq. (Suppl.) (1976).

[6] The Sommerfeld Parameter is an estimate of conditions for classical behavior. $\eta = a/\lambda_0 >> 1$, where a is the dimension of interaction and λ_0 the wavelength at infinity for the system. See A. Messiah, Quantum Mechanics, Vol. 1 North Holland Publishing Co., Amsterdam, p. 214ff (1961).

[7] J. V. Kratz, A. E. Norris, and G. T. Seaborg, Phys. Rev. Lett. 33, 502 (1974).

[8] R. J. Otto, M. M. Fowler, D. Lee, and G. T. Seaborg, Phys. Rev. Lett. 36, 135 (1976).

[9] H. H. Deubler and K. Dietrich, Phys. Lett. 62B, 369 (1976).

[10] R. Bimbot, and M. F. Rivet, Phys. Rev. C 8, 375 (1973).

[11] L. G. Moretto, B. Cauvin, P. Glassel, R. Jared, P. Russo, J. Sventeck and G. Wozniak, Phys. Rev. Lett. 36, 1069 (1976).

[12]P. Russo, R. P. Schmitt, G. J. Wozniak, R. G. Jared, P. Glässel, B. Cauvin, J. S. Sventeck, and L. G. Moretto, Nucl. Phys. A281, 509, (1977).

[13]P. Russo, B. Cauvin, P. Glässel, R. C. Jare,d R. P. Schmitt, G. J. Wozniak, and L. G. Moretto, Phys. Lett. 67B, 155 (1977).

[14]I. Binder, Ph.D. thesis, University of California Berkeley (1977) Lawrence Berkeley Laboratory Report, LBL 6515.

[15]L. C. Northcliffe, R. G. Schilling, Nucl. Data Sect. A7, 233)1970).

[16]A. Ghiorso (private communication, 1977).

[17]R. Vandenbosch, M. P. Webb, and T. D. Thomas, Phys. Rev. Lett. 36, 549 (1976).

[18]R. Vandenbosch, M. P. Webb, and T. D. Thomas, Phys. Rev. C 14, 143 (1976).

[19]W. U. Schröder, J. R. Birkelund, J. R. Huizenga, K. L. Wolf, J. P. Unik, and V. E. Viola, Phys. Rev. Lett. 36, 514 (1976).

[20]R. Vandenbosch, M. P. Webb, T. D. Thomas, and M. S. Zisman, Nucl. Phys. A263, 1 (1976).

[21]K. Dietrich (private communication, 1977).

TABLE I. Summary of recoil range experiments and bombarding conditions.

Projectile and target	E_p (MeV)[b]	$\frac{E-B}{B}$[c]	η'	Average beam intensity (particles/sec)	Target thickness (mg/cm^2)
$^{86}Kr + {}^{197}Au$	581	0.43	351	1×10^{10}	2.32
$^{86}Kr + {}^{197}Au$	491	0.22	587	1×10^{10}	2.32
$^{86}Kr + {}^{197}Au$	420	0.04	1076	1×10^{10}	2.32
$^{136}Xe + {}^{197}Au$	868	0.29	561	4×10^{9}	2.32
$^{86}Kr + {}^{238}U$[a]	686	0.58	304	4×10^{10}	1.01[d]

[a]Nonparasitic experiment.

[b]Average energy of projectile in target.

[c]B was calculated using $R = (1.225(A_1^{\frac{1}{3}} + A_2^{\frac{1}{3}}) + 2)\text{fm}$.

[d]mg/cm^2 of uranium as UF_4.

TABLE II. Calculated ranges for quasitarget fragments.

Reaction	E_p (MeV)	Grazing angle (degrees)[a] projectile c.m.s	Grazing angle (degrees)[a] projectile lab	Target lab	Fragment	Fragment ranges (mg/cm^2 of Al) R_{max}	R_{min}	R_{90}	R_g
$^{86}Kr + ^{197}Au$	581	64	46	57	^{191}Pt	7.5	-0.89	3.7	2.3
$^{86}Kr + ^{197}Au$	491	89	65	46	^{191}Pt	7.1	-0.98	3.3	3.3
$^{86}Kr + ^{197}Au$	420	136	113	22	^{191}Pt	6.7	-1.0	3.1	5.7
$^{136}Xe + ^{197}Au$	868	78	47	51	^{197}Au	11.5	-0.81	5.2	4.2
		54			^{187}Re	12.1	-0.95	5.2	4.0
$^{86}Kr + ^{238}U$	686	54	41	63	^{199}Au	8.6	-1.1	3.6	1.3

[a]The grazing angle was calculated using

$$\cot(\theta_{grazing}) = (2R/b)-1 \quad \text{where } R = 1{,}225(A^{\frac{1}{3}} + A_2^{\frac{1}{3}}) + 2 \text{ fm and } b = e^2 Z_1 Z_2 / E_{c.m.s.}.$$

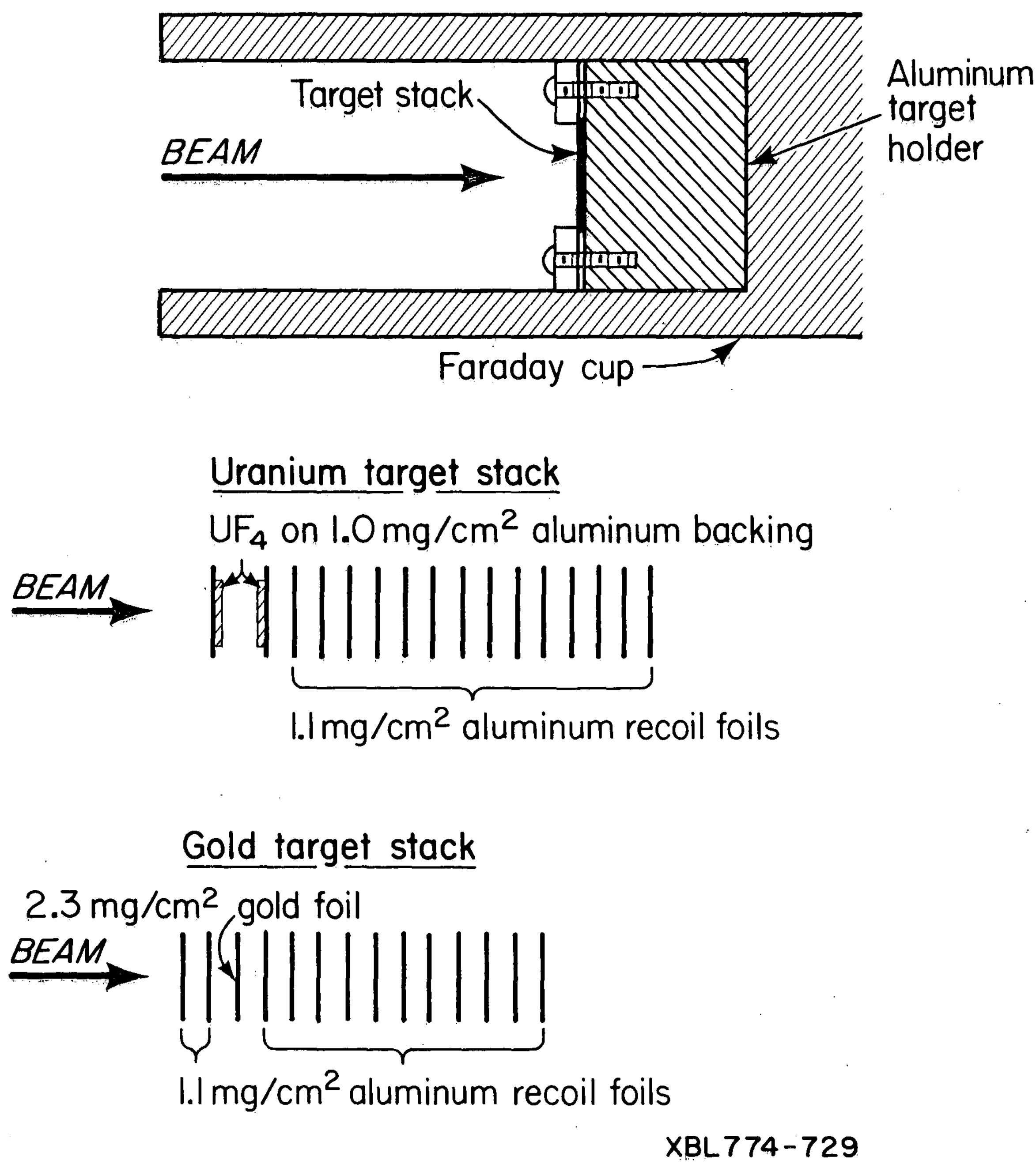

Fig. 1. Diagram of recoil target and recoil catcher foils holder.

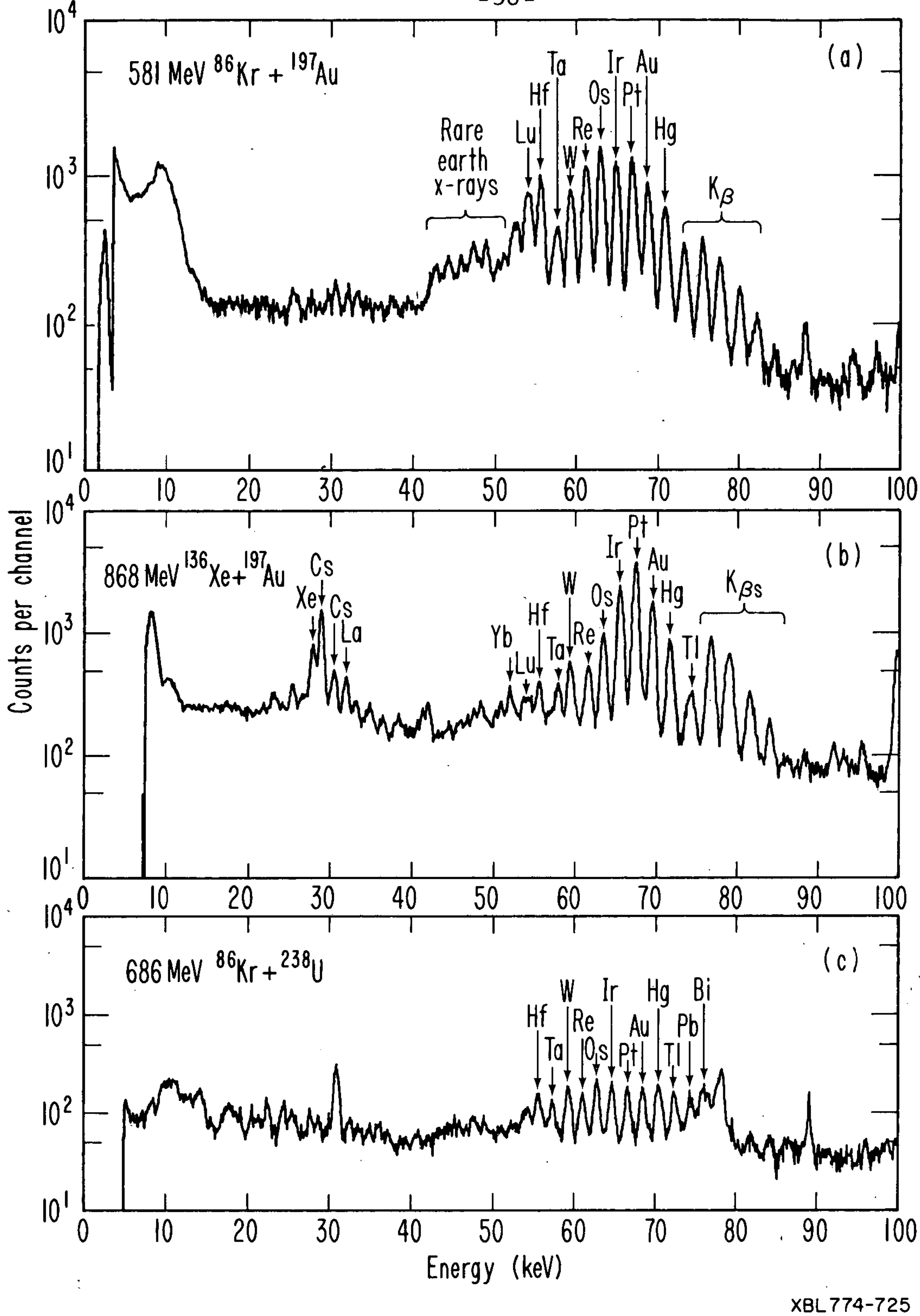

Fig. 2. X-ray spectra from the third aluminum recoil catcher foil in each of three experiments. Each x-ray peak in the region between 50 and 70 keV is composed of the $K_{\alpha 1}$ x ray from the element shown above the peak and the $K_{\alpha 2}$ x ray from the element one atomic number larger. The higher energy K_β x rays associated with the x-ray peaks in the region between 60 and 70 keV are noted.

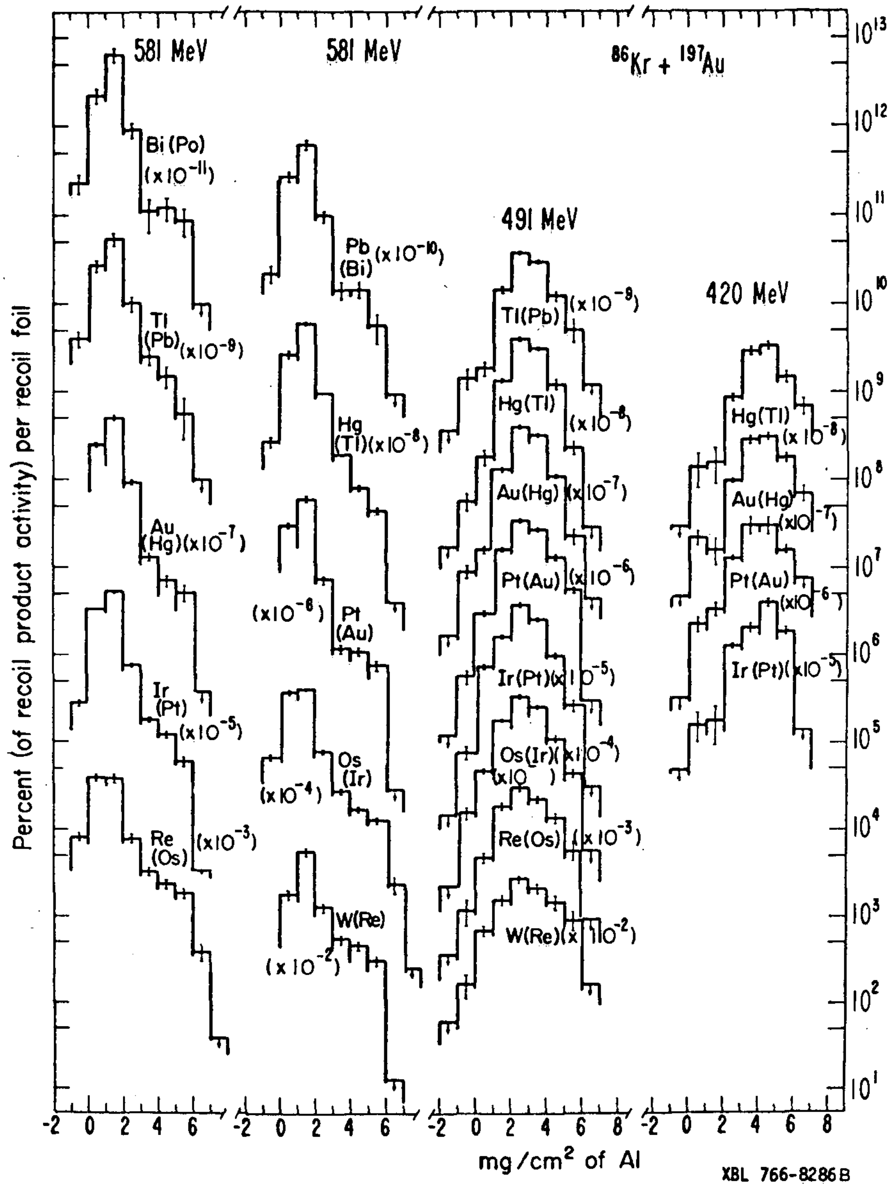

Fig. 3. Experimental recoil range distribution for the reaction of ^{86}Kr with ^{197}Au at the three energies shown in the figure. Each range distribution is for the elements shown to the right or below the distribution. The range distributions are based on individual x-ray peaks composed of the $K_{\alpha 1}$ x ray from the element indicated (not in parenthesis) and the $K_{\alpha 2}$ x ray from the element of the next higher atomic number shown in parenthesis. See text for further explanation of axes.

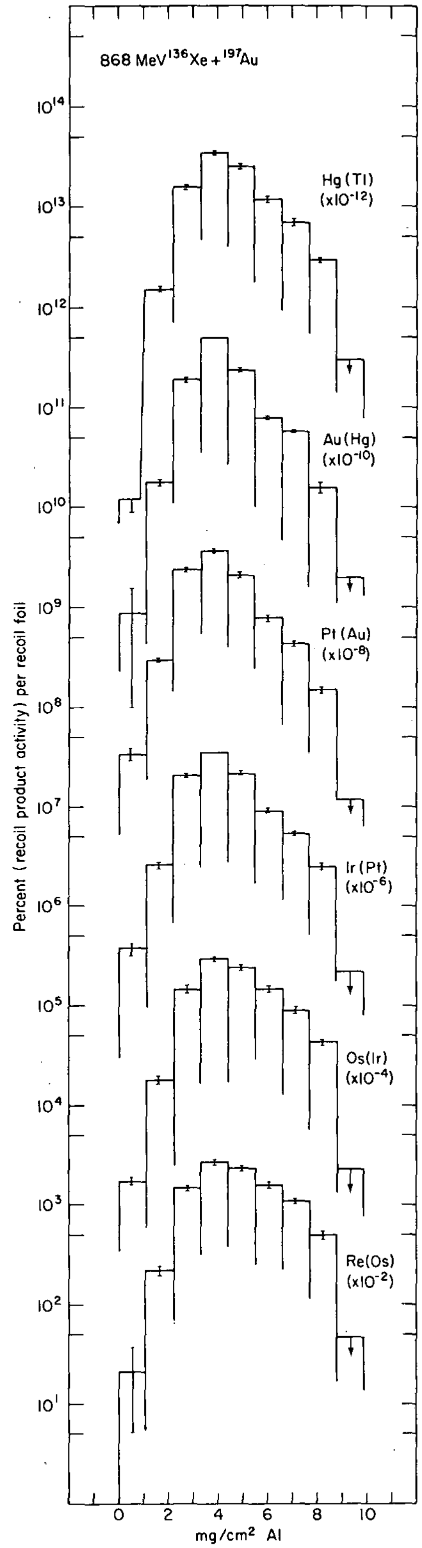

Fig. 4. Experimental recoil range distributions for the reaction of 868 MeV ^{136}Xe + ^{197}Au. See text and Fig. 3 caption for further explanation.

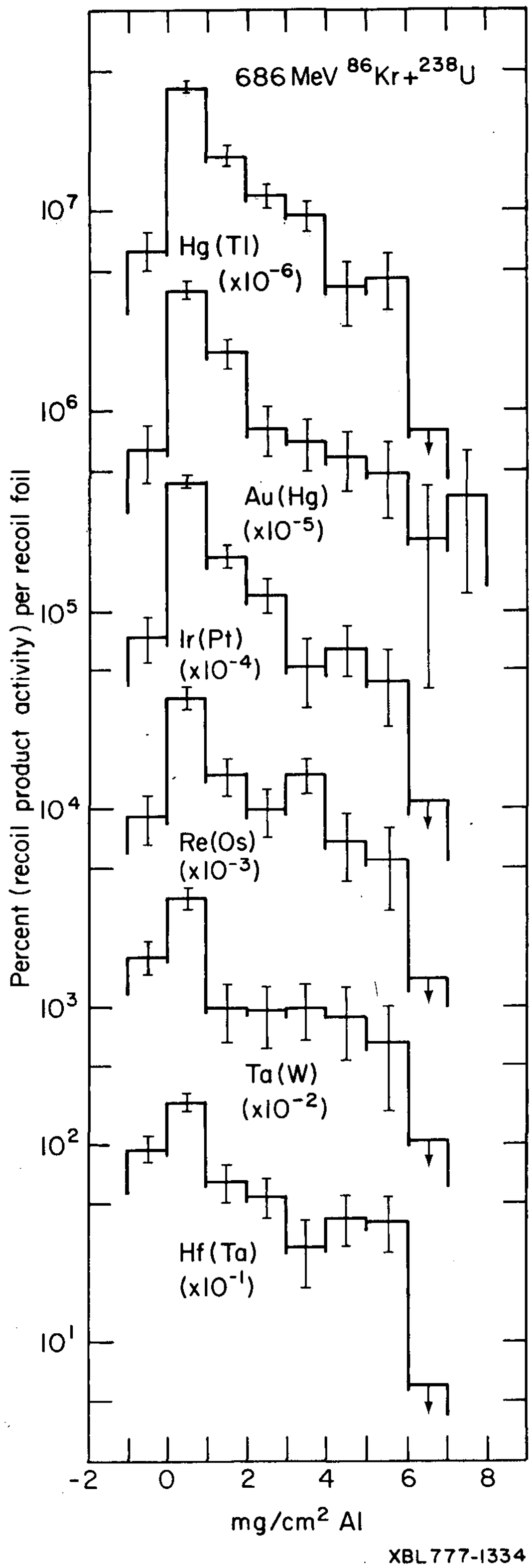

Fig. 5. Experimental recoil range distributions for the reaction of 686 MeV ^{86}Kr + ^{238}U. See text and Fig. 3 caption for further explanation.

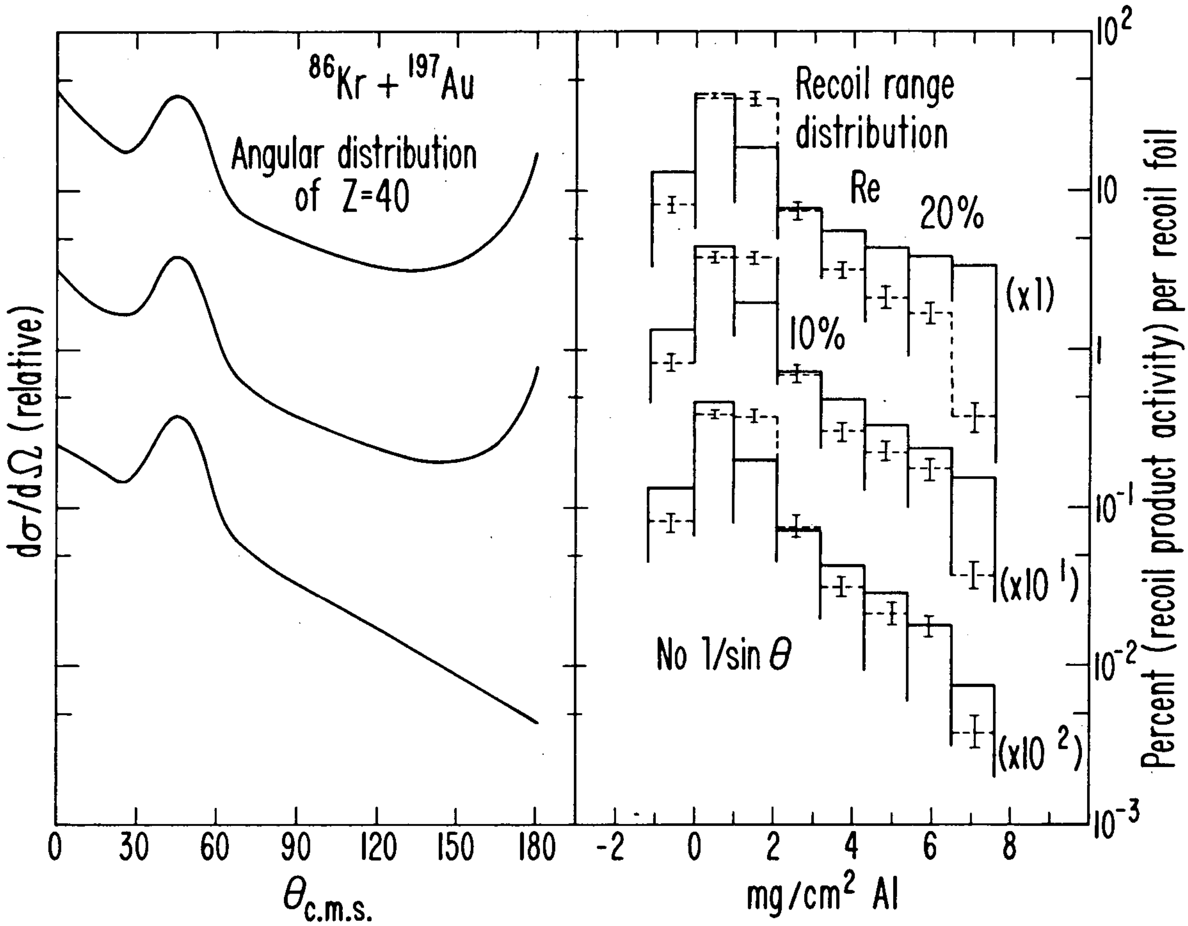

XBL 774-732

Fig. 6. Experimental and calculated recoil range distributions for Re(Os) products for the reaction of 581 MeV ^{86}Kr + ^{197}Au. The range distributions shown as solid lines were calculated using the fully damped model and the hypothetical angular distributions for the complementary projectile-like fragment shown to the left of the range distribution. The experimental range distributions are shown as dotted lines with error bars. The percentages in the figure on the right indicate hypothetical percentages of 1/sin θ contribution to the reaction and angular distributions shown to the left.

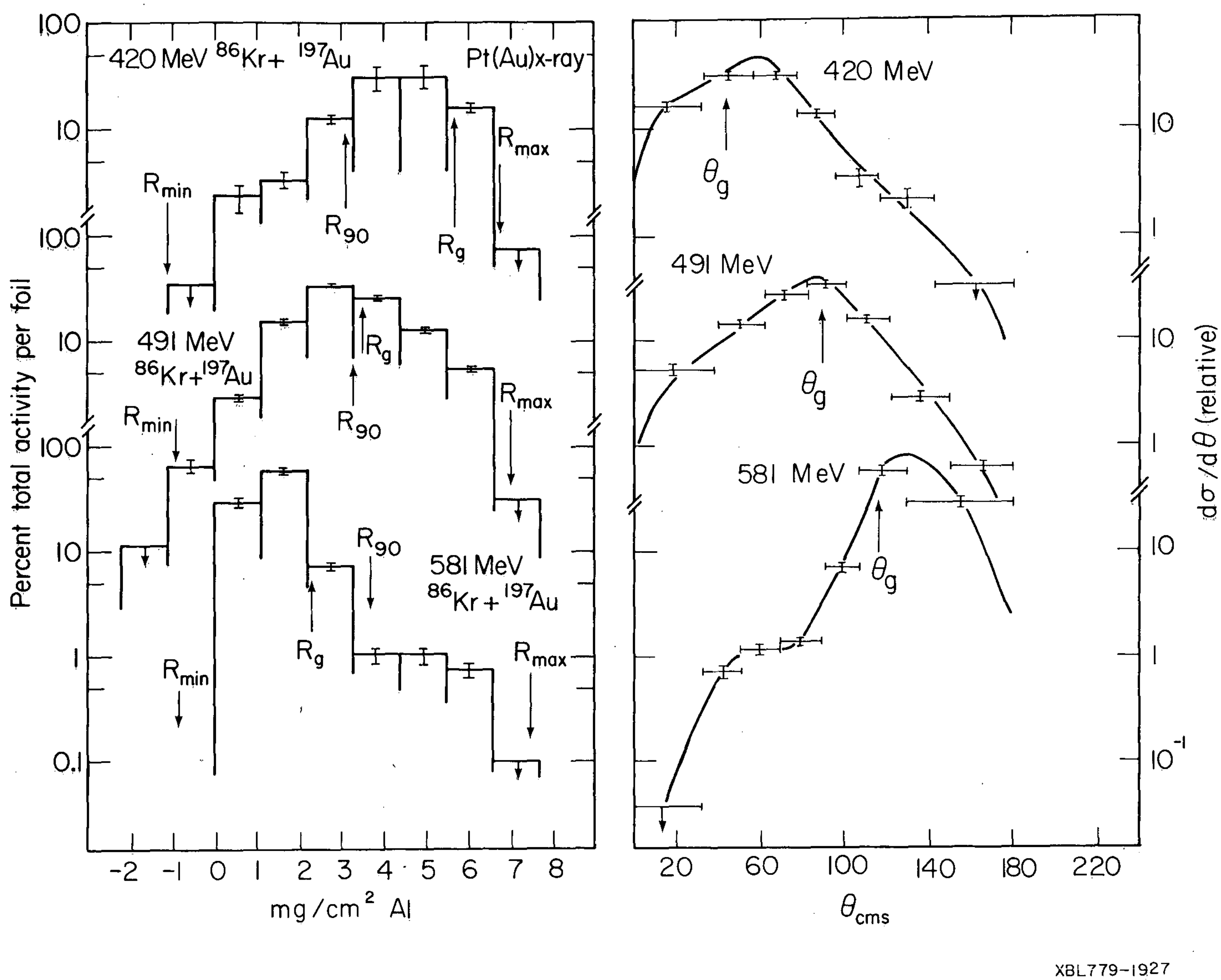

Fig. 7. Comparison of the recoil range distribution for the reaction of ^{86}Kr with ^{197}Au at three different energies. The range distributions were obtained from the measured x-ray peak areas composed of the Pt $K_{\alpha 1}$ x ray and the $Au_{\alpha}K_2$ x ray. See text for explanation of axes and R_{min}, R_g, R_{90}, and R_{max}. Shown to the right are the angular distributions for the same products calculated from the recoil range data.

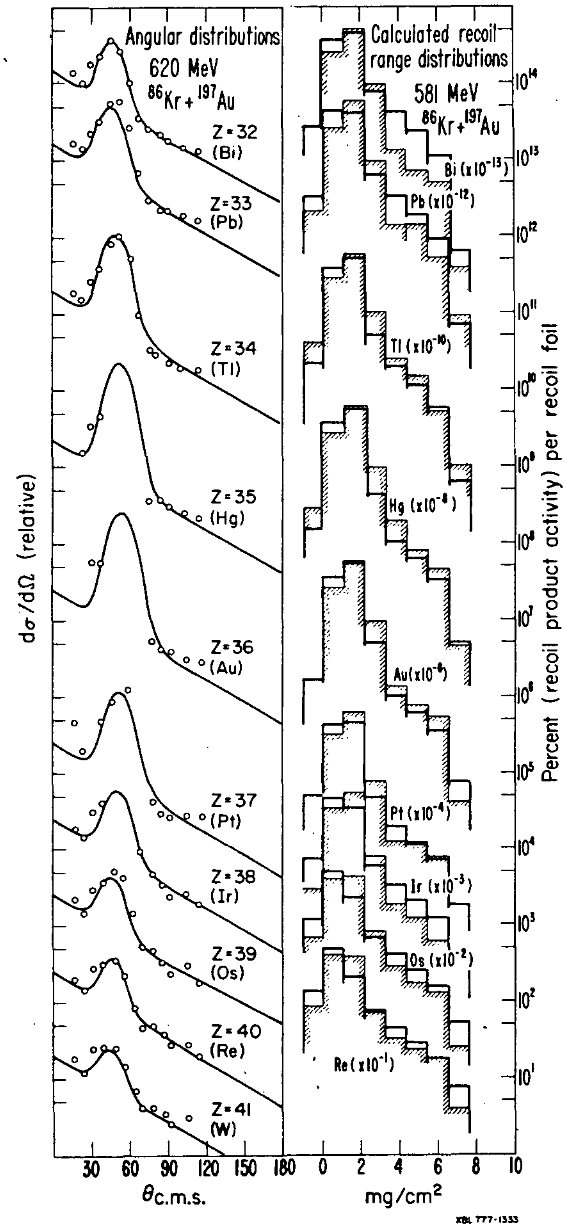

Fig. 8. Calculated range distributions (solid lines on right) for the reaction of 581 MeV ^{86}Kr + ^{197}Au. The range distributions were calculated using the fully damped model and the angular distributions of the complementary light fragment (shown to the left) from 620 MeV ^{86}Kr + ^{197}Au[11,12]. The shaded regions represent the experimental recoil range distributions for each element (see Fig. 3).

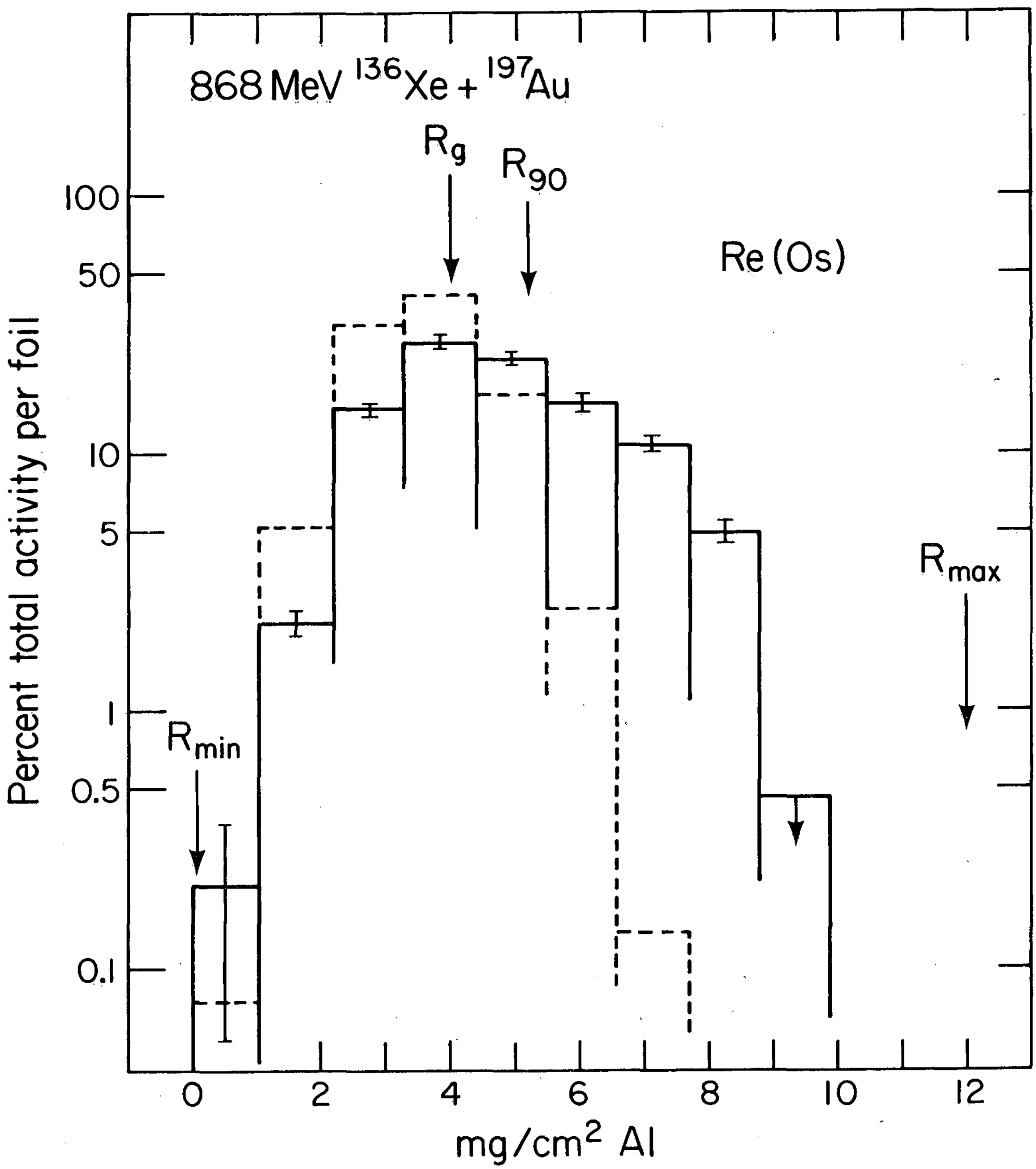

XBL 774-731

Fig. 9. Calculated recoil range distribution for the element Re(Os) produced in the reaction of 868 MeV ^{136}Xe + ^{197}Au. The calculated recoil range distribution is shown as a dotted line and the experimental range distribution for the same element is shown as a solid line. See text for explanation of axes and R_{min}, R_g, R_{90}, and R_{max}.

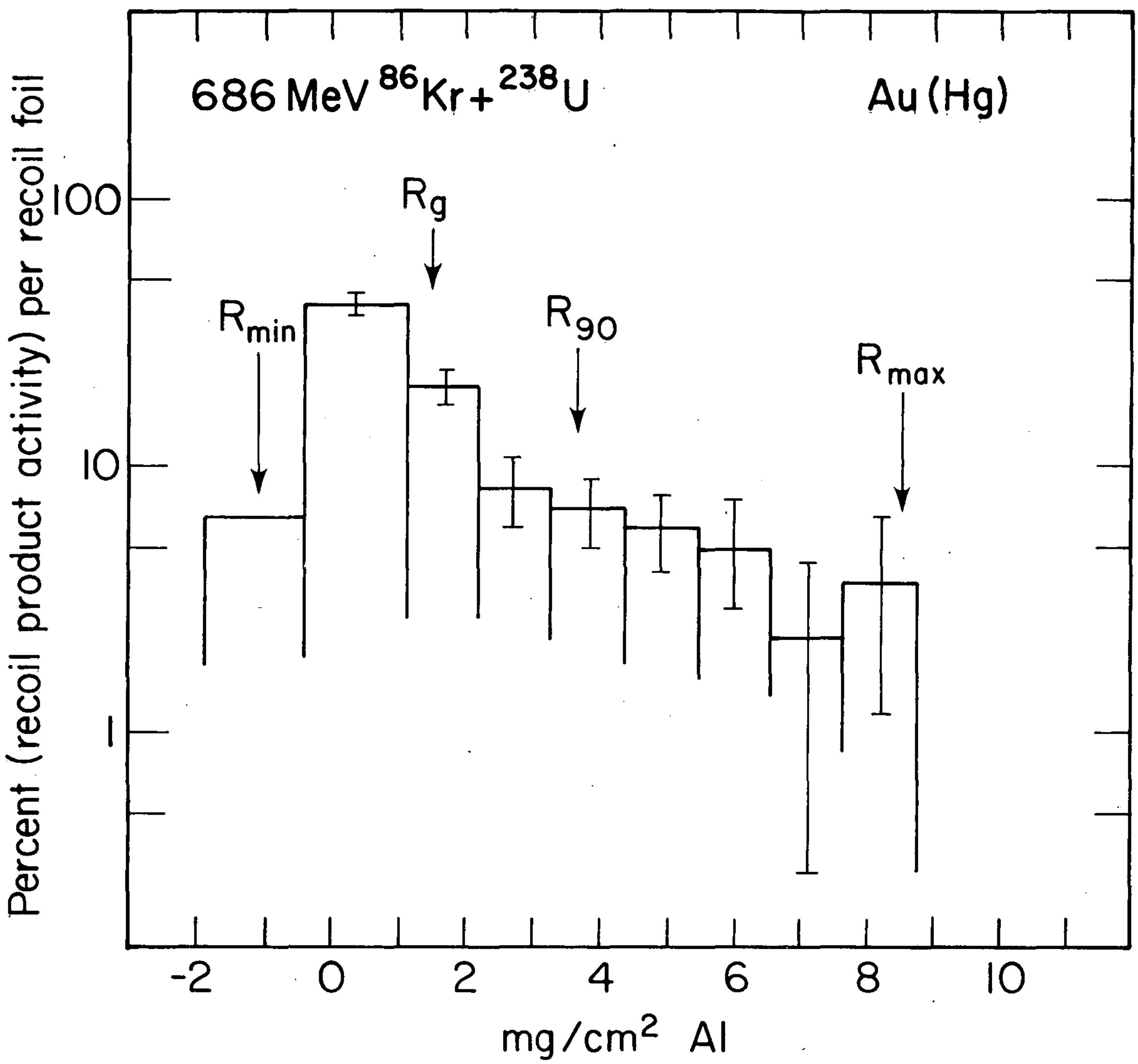

XBL 777-1335

Fig. 10. Comparison of the experimental recoil range distribution for the reaction of 686 MeV $^{86}Kr + ^{238}U$. The recoil range distributions were obtained from the measured x-ray peak areas composed of the Au $K_{\alpha 1}$ x ray and the Hg $K_{\alpha 2}$ x ray. See text for explanation of axes and R_{min}, R_g, R_{90}, and R_{max}.

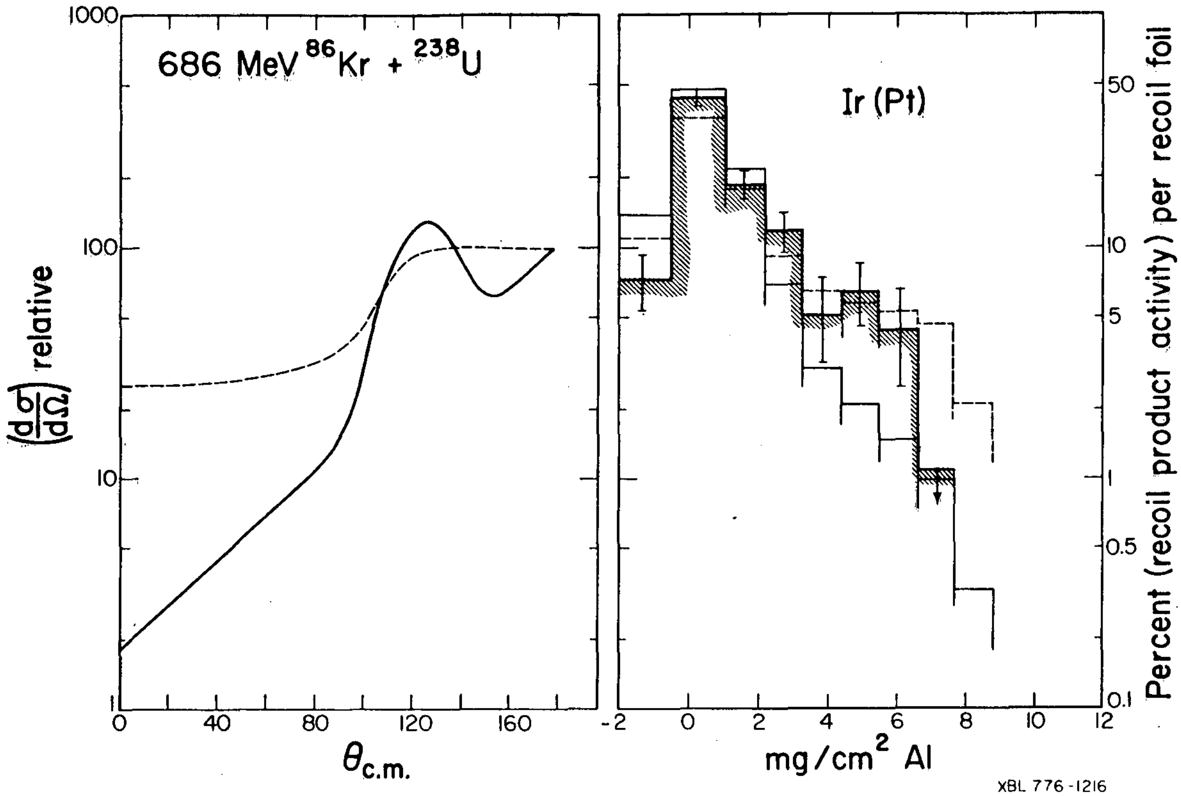

Fig. 11. Comparison of experimental and calculated recoil range distributions for the Ir(Pt) products formed in the reaction of 686 MeV ^{86}Kr + ^{238}U. The shaded distribution shown with error bars is the experimental axial recoil range distribution. The angular distributions shown to the left as solid and dotted lines were used to calculate the theoretical range distributions on the right also shown as solid and dotted lines as explained in the test.

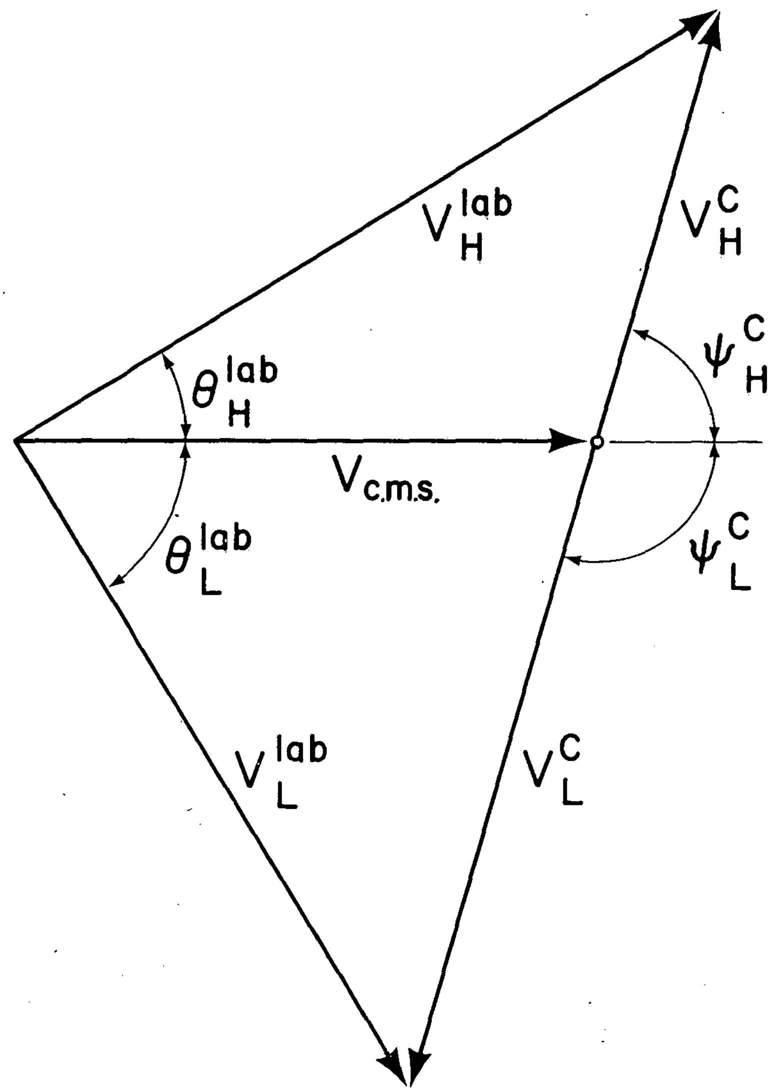

XBL 776-1215

Fig. 12. Velocity vector diagram of the simplified reaction model used.

This report was done with support from the Department of Energy. Any conclusions or opinions expressed in this report represent solely those of the author(s) and not necessarily those of The Regents of the University of California, the Lawrence Berkeley Laboratory or the Department of Energy.

TECHNICAL INFORMATION DEPARTMENT
LAWRENCE BERKELEY LABORATORY
UNIVERSITY OF CALIFORNIA
BERKELEY, CALIFORNIA 94720